Energy Management Strategy for HEVs Including Battery Life Optimization

Li Tang, *Member, IEEE*, Giorgio Rizzoni, *Fellow, IEEE*, and Simona Onori, *Member, IEEE*

***Abstract*—This paper presents an optimal control-based energy management strategy for a parallel hybrid electric vehicle (HEV). Not only does this strategy try to minimize fuel consumption while maintaining the state of charge of the battery within reasonable bounds, it also seeks to minimize wear of the battery and extend its life. This paper focuses on understanding the optimal control solution offered by Pontryagin's minimum principle (PMP) in this context. Simulation-based results are presented and analyzed, which show that the control algorithm is able to reduce battery wear by decreasing battery operating severity factor with minimal fuel economy penalty. The benefit of this strategy is especially evident when ambient and driving conditions are especially severe.**

***Index Terms*—Battery aging, energy management, hybrid electric vehicle (HEVs), optimal control, Pontryagin's minimum principle (PMP).**

I. Introduction

HYBRID electric vehicles (HEVs) represent a steadily increasing segment of the automotive market. The fuel economy of HEVs is highly dependent on the energy capacity of the on-board energy storage system. However, these energy storage systems experience degradation in both energy capacity and internal resistance due to several irreversible degradation processes. The rate of battery capacity loss is dictated by many factors including operating and environmental conditions. Factors such as extreme temperature, high C-rate, high or low state of charge (SOC), and excessive depth of discharge are recognized to contribute to capacity degradation [1]–[5]. Li-ion batteries represent a big part of vehicle cost. Hence, designing batteries to last for the life of a vehicle while still satisfying the energy and power requests is a requirement. An HEV equipped with a supervisory energy management controller that is able to reduce the battery aging effects during vehicle operation can potentially extend the battery life and reduce overall cost.

However, limiting stresses on the battery that could accelerate its aging may result in energy management policies that are in conflict with the desire to minimize fuel consumption. Mathematically, this situation can be described as a multiobjective optimization problem. In [6], the authors propose an energy management strategy for a power split plug-in hybrid electric vehicle (PHEV) with consideration of battery health that is represented by an electrochemical model describing anode-side solid electrolyte interphase (SEI) growth, which only captures a certain aspect contributing to battery aging. In [7], the authors proposed a multiobjective optimal control problem, which consider both fuel consumption and battery aging by converting battery pack replacing cost to equivalent fuel cost. The major limitation of [7] is that the authors use the postulated aging model provided by the manufacture instead of an experimental validated model. The idea in this paper is inspired by [7] and significantly extends these results. In [8], instead of considering battery aging explicitly in the objective function, the authors treat battery state of health (SOH) as one of the states. Due to the fact that the time scales of battery SOC and SOH are separated by more than three orders of magnitude, two separate controllers are used to regulate the two states by tracking the set points. However, an optimal solution is not presented, so the connection or real tradeoff between battery life span and fuel economy is not fully explored. Given the fact that temperature is an essential impact factor on battery life, the authors of [9] impose a penalty on battery temperature, which is supposed to represent the cost of battery health. However, high C-rate will stress the battery even at mild temperature. In addition, it is very difficult to quantify the actual amount of Ah-throughput, which is related to battery life, saved by this strategy due to the lack of an appropriate aging model. To properly address the tradeoff between fuel consumption and battery life, it is necessary to develop an aging model that is able to capture all the important factors related to the battery aging process.

In this paper, the energy management problem in HEVs is formulated as an optimal control problem in which the control algorithm is required to tradeoff between two objectives: 1) minimizing fuel consumption and 2) minimizing battery degradation. To find a solution to this problem, we use a battery capacity degradation model that considers the battery Ah-throughput as a measure of battery life; the model is parameterized using experimental data that correspond to HEV driving conditions. This optimal control problem is solved by the Pontryagin's minimum principle (PMP). Simulation-based results are presented and analyzed to evaluate the benefits of the strategy. The main contribution of this work is that a control-oriented and experimental validated battery capacity degradation model is linked to an energy management problem for HEVs. The optimal solution provides important insights into the interdependency of battery aging and energy management, and permits exploration of tradeoffs between fuel economy and battery capacity loss, the regenerative braking strategy, and the

Manuscript received April 08, 2015; revised July 31, 2015; accepted August 05, 2015. Date of publication August 21, 2015; date of current version October 15, 2015. This work was supported in part by Honda R&D Co., Ltd, and in part by Automobile R&D Center, Tochigi, Japan.

L. Tang and G. Rizzoni are with the Center for Automotive Research, Department of Mechanical and Aerospace Engineering, Ohio State University, Columbus, OH 43212 USA (e-mail: tang.437@osu.edu).

S. Onori is with the Department of Automotive Engineering, Clemson University, Greenville, SC 29607-5257 USA.

Color versions of one or more of the figures in this paper are available online at http://ieeexplore.ieee.org.

Digital Object Identifier 10.1109/TTE.2015.2471180

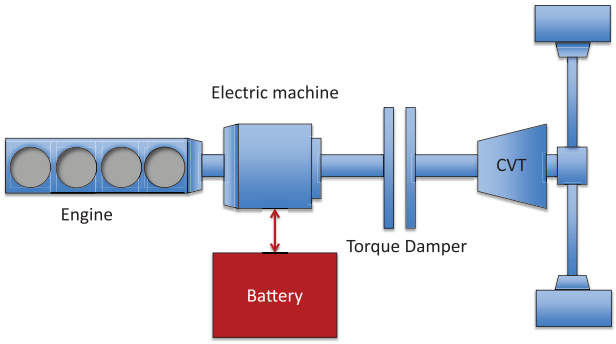

Fig. 1. Vehicle architecture.

TABLE I
SPECIFICATIONS OF VEHICLE COMPONENTS

Components	Specification
Vehicle mass	1294 kg
IC engine	1.6 liter 85 kW gasoline engine
Electric machine	Peak power 30 kW, continuous 15 kW
CVT	Ratio: 3.172–0.529, final drive: 3.94
Battery pack	Li-ion 820 Wh, 4.6 Ah, 20 kW

sizing of components, which shows the potential of improving overall performance while reducing the cost. The optimal strategy illustrates the ability to significantly extend battery life without unduly affecting fuel economy especially under harsh driving conditions.

This paper is organized as follows. In Section II, the model of a parallel HEV and its Simulink implementation are presented. In Section III, the problem formulation is presented, and expressions of the analytical solution provided by PMP are described. The regenerative braking strategy is presented in Section IV, which is followed by engine start–stop in Section V. Section VI describes the implementation of the optimal controller, and in Section VII, the results obtained from simulations are interpreted and analyzed to provide insights into the control algorithm.

II. VEHICLE MODEL

A. System Description

The system analyzed in this paper is a parallel pretransmission hybrid, which is shown in Fig. 1. The main characteristics of the components are listed in Table I. The internal combustion engine is a 1.6-L naturally aspirated inline four-cylinder gasoline engine. The electric drive system allows for both power assist and battery charging, as well as regenerative braking. The engine and electric machine are mounted on the same shaft which connects to the continuous variable transmission (CVT) through a torque damper. The powertrain is modeled using a quasi-static forward approach [10]. The desired vehicle velocity is the input signal from the driving cycle. Following the speed profile, the driver, which is modeled as a PI controller, gives commands on acceleration and braking. The CVT ratio is generated accordingly. A supervisory control algorithm sets the power split between the electric machine and the internal

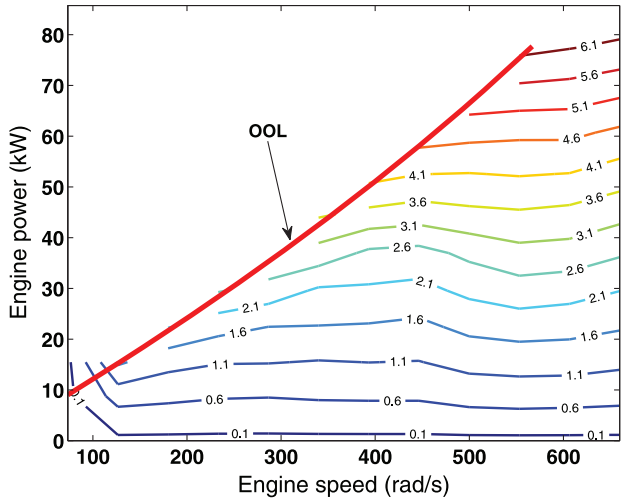

Fig. 2. Engine optimal operation line.

combustion (IC) engine. In this work, the control input $u(t)$ is chosen to be the power of the electric machine $P_{\mathrm{em_{req}}}$. This power is subjected to speed-dependent constraints

$$u(t) = P_{\mathrm{em_{req}}} \in [P_{\mathrm{em,min}}(\omega_{\mathrm{em}}), P_{\mathrm{em,max}}(\omega_{\mathrm{em}})] \quad (1)$$

where $\omega_{\mathrm{em}}(t)$ is the rotational speed of the electric machine, which is known. In addition to the physical limits of both actuators, the power request from the driver should always be satisfied. Both the engine data and electric machine data are from Powertrain System Analysis Toolkit (PSAT).

B. Engine

The fuel flow rate of the engine is given by a steady-state map, which is a function of engine torque T_{ice} and engine speed ω_{ice}, i.e., $\dot{m}_f = f(\omega_{\mathrm{ice}}, T_{\mathrm{ice}})$. The power consumption of the engine can be described by equation

$$P_{\mathrm{fuel}} = \mathrm{LHV} \cdot \dot{m}_f \quad (2)$$

in which LHV is the lower heating value of the fuel.

C. Electric Machine

The efficiency of the electric machine η_{em} is given by a steady-state map, which is a function of both torque T_{em} and speed ω_{em}. Therefore, the power request of the electric machine is given by the torque, in which $z = -1$ when the electric machine works as a motor, and $z = 1$ when it works as a generator

$$P_{\mathrm{em_{req}}} = T_{\mathrm{em}} \cdot \omega_{\mathrm{em}} \cdot \eta_{\mathrm{em}}^{z}(\omega_{\mathrm{em}}, T_{\mathrm{em}}). \quad (3)$$

D. Transmission

A CVT is used to keep the internal combustion engine operating at low fuel consumption points by tracking the optimal operation line (OOL) [11], which is shown in Fig. 2. The OOL can be calculated from the engine map by minimizing the fuel

consumption for a set of power outputs. Based on the OOL, the optimal engine speed for a given throttle position, which is equivalent to the angle of the acceleration pedal, can be decided. The OOL tracking strategy is implemented as a 2-D look-up table. Thus, CVT ratio is not considered as a part of the optimization. Due to the fact that the architecture of the vehicle model is parallel pretransmission hybrid, the CVT ratio is determined before the torque split. As a result, the engine will operate around the OOL instead of being exactly on the OOL.

E. Battery

The battery is modeled by an equivalent circuit comprising a voltage source $V_{\rm oc}$ and its internal resistance R_0 in series, and both variables are functions of the SOC. Thus, the battery current is given by [7]

$$I_{\rm batt} = \frac{V_{\rm oc} - \sqrt{V_{\rm oc}^2 - 4 \cdot R_0 \cdot P_{\rm batt}}}{2 \cdot R_0} \tag{4}$$

in which $P_{\rm batt}$ is the power in and out of the battery. SOC is computed from the battery current as

$$\mathrm{SOC}(t) = \mathrm{SOC}_0 - \frac{1}{Q_{\rm batt}} \cdot \int_0^t I_{\rm batt}(\tau) d\tau \tag{5}$$

in which $Q_{\rm batt}$ is the battery capacity.

In addition to SOC, battery temperature is also a state of the battery system model. However, in the optimal control system, temperature is not considered as a state assuming that an independent battery thermal management system will keep the battery temperature at a known desired value.

F. Battery Aging

Aging models for lithium-ion batteries can be classified into two categories, namely physical–chemical models and empirical models. Physical–chemical models are usually developed to study or describe a single aging mechanism inside the cell [12], [13]. For instance, a first-principles capacity fade model is developed based on the mechanism for SEI growth [14]. This type of models are helpful in understanding of aging under different modes as well as the effect of an aging source on different aspects of the cell performance. Such first-principles models have limitations such as the requirement of a detailed model of the aging processes and often require long computation time. To remedy these shortcomings, various empirical and semiempirical models have been proposed [15], [16]. These models are developed by considering simplified physical relations in the model by fitting the parameters of the model with experimental data obtained from aging tests, resulting in a set of equations that describe the main degradation mechanisms. Due to the favorable compromise between simplicity and accuracy, semiempirical models are employed in the control-oriented models used in this study. We start from a generic model initially proposed in [5], which has the form

$$Q_{\rm loss} = B \cdot \exp\left(\frac{-E_a}{R \cdot \theta}\right) \cdot (\mathrm{Ah})^z \tag{6}$$

TABLE II
BATTERY AGING EXPERIMENT DATA

Data	$\bar{\mathrm{SOC}}$ [%]	$\bar{I}_c[1/h]$	$\bar{\theta}$[°C]
Profile A	38.5	2.8	36
Profile B	42.0	3.0	38
Profile C	68.0	6.0	45

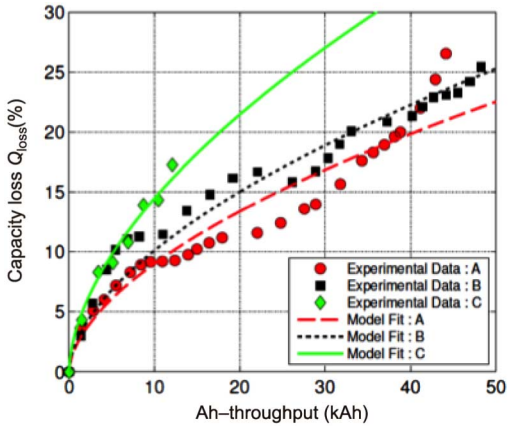

Fig. 3. Curve fitting result of identified aging model with the experimental data [19].

where $Q_{\rm loss}$ is the battery capacity loss in percentage with respect to the nominal capacity, B is a preexponential factor, E_a is the activation energy in $\mathrm{J} \cdot \mathrm{mol}^{-1}$, R is the gas constant, θ is the battery temperature expressed in Kelvin, Ah is the Ah-throughput, and z is the power law factor. In order to capture the battery aging effects under HEV operating conditions as well as to incorporate dependence on SOC, the generic aging model is calibrated on battery aging data obtained from a charge sustaining HEV, and the data are reported in Table II where profiles A and B are from [17] and profile C is from [18]. The three profiles use the same type of battery, which is $\mathrm{LiFePO_4}$ cell (ANR26650) from A123 system, and are specified in terms of average $\bar{\mathrm{SOC}}$, average C-rate $\bar{I}_c$, and average battery temperature $\bar{\theta}$. Following a two-step curve fitting procedure, the result is shown in Fig. 3 and the identified aging model [19] has the form of

$$Q_{\rm loss\%} = (\alpha \cdot \mathrm{SOC} + \beta) \cdot \exp\left(\frac{-31700 + 163.3 \cdot I_c}{R \cdot \theta}\right) \cdot \mathrm{Ah}^{0.57} \tag{7}$$

$$\alpha = \begin{cases} 1287.6, & \mathrm{SOC} \leqslant 0.45 \\ 1385.5, & \mathrm{SOC} > 0.45 \end{cases}$$

$$\beta = \begin{cases} 6356.3, & \mathrm{SOC} \leqslant 0.45 \\ 4193.2, & \mathrm{SOC} > 0.45. \end{cases}$$

III. PROBLEM FORMULATION

The problem we consider in this paper is the energy management of a charge-sustaining HEV. In the vehicle architecture considered in this study, we consider three distinct operating modes: 1) charge sustaining hybrid mode; 2) braking regeneration mode; and 3) engine start–stop. Each of these modes

affects both the fuel economy of the vehicle and the life of the battery. We focus the optimal control problem formulation on the charge-sustaining mode, and we treat the other two problems separately, for the following reasons. Engine start–stop is modeled by a simple rule base, described later in this section and representative of current industrial practice, which leads to the computation of a fixed cost (electricity and fuel) for each engine restart (assuming warmed-up engine). This choice is appropriate for the architecture considered in the study, which is based on the Honda Civic HEV, and in which no electric launch function or pure electric driving is considered. In a different HEV architecture, or in a PHEV, one would have the freedom to delay the start of the engine, having the ability to rely on a more substantial electrical energy buffer. Selecting the engine start time would then lead to a mixed-integer optimal control problem—we do not address this problem here, although it presents an interesting extension of our work. Braking regeneration is also very important, as there is a clear tradeoff between recovering as much energy as possible and limiting the aging of the battery. Since the decision to apportion electromechanical versus friction braking is an instantaneous one, in this paper, we have formulated the braking regeneration aging-fuel economy tradeoff as a static optimization problem which is solved separately.

The objectives of the optimal control problem formulated and solved in this paper are twofold: minimizing fuel consumption, while minimizing battery capacity degradation. A crucial step in formulating such optimal control problem consists in the development of a model to properly quantify the battery wear to be included in the cost function. It is clear that operating conditions dictate battery aging phenomena, so different battery life durations are expected when the battery is operated under different inputs. The concept of severity factor is utilized to quantify the relative aging effect with respect to a nominal operating condition. If the end of life of a battery is defined as 20% capacity drop from its initial value, then battery life with respect to a nominal cycle can be characterized by the total Ah-throughput when the battery reach the end of life [20], [21]. The nominal battery life Γ can be expressed as

$$\Gamma = \int_0^{\mathrm{EOL}} |I_{\mathrm{nom}}(t)| dt \tag{8}$$

where I_{nom} is the current profile under nominal conditions.

The relative aging effects of any other load cycle the battery is subject to can be reflected by severity factor

$$\sigma(I, \theta, \mathrm{SOC}) = \frac{\Gamma}{\gamma(I, \theta, \mathrm{SOC})} = \frac{\int_0^{\mathrm{EOL}} |I_{\mathrm{nom}}(t)| dt}{\int_0^{\mathrm{EOL}} |I(t)| dt} \tag{9}$$

where $\gamma(I, \theta, \mathrm{SOC})$ is the battery life given in terms of Ah-throughput corresponding to specific operating conditions given in terms of current I, temperature θ, and SOC [20], [21]. When the battery is undergoing a more severe load cycle, the severity factor is greater than one and a shorter life is expected. The concept of severity factor to express the relative aging effect of a specific load cycle was proposed in [20] and [22].

The severity factor σ can be obtained empirically using the aging model in (7). The end of life is defined as 20% loss of capacity and the nominal conditions defined in this study are $I_{c,\mathrm{nom}} = 2.5, \mathrm{SOC}_{\mathrm{nom}} = 0.35$, and $\theta_{\mathrm{nom}} = 25\,^{\circ}\mathrm{C}$, then the nominal battery life Γ can be calculated as

$$\Gamma = \left[\frac{20}{(\alpha \cdot \mathrm{SOC}_{\mathrm{nom}} + \beta) \cdot \exp\left(\frac{-31700 + 163.3 \cdot I_{c,\mathrm{nom}}}{R \cdot \theta_{\mathrm{nom}}} \right)} \right]^{\frac{1}{0.57}}. \tag{10}$$

Battery life under different load conditions can be followed as

$$\gamma = \left[\frac{20}{(\alpha \cdot \mathrm{SOC} + \beta) \cdot \exp\left(\frac{-31700 + 163.3 \cdot I_c}{R \cdot \theta} \right)} \right]^{\frac{1}{0.57}}. \tag{11}$$

Severity factor is ready to be calculated by taking the ratio of Γ and γ obtained from (10) and (11).

In order to give the effective life depletion due to charge exchange within the battery, we define effective Ah-throughput as [21]

$$\mathrm{Ah}_{\mathrm{eff}}(t) = \int_0^t \sigma(I_c, \theta, \mathrm{SOC}) \cdot |I(\tau)| d\tau. \tag{12}$$

Effective Ah-throughput gives the effective life depletion with respect to the nominal life defined by Γ. Thus, the battery will reach the end of life when $\mathrm{Ah}_{\mathrm{eff}}(t) = \Gamma$, and the objective of minimizing battery aging is equivalent to minimizing $\mathrm{Ah}_{\mathrm{eff}}(t)$ [7].

Considering fuel economy and battery aging simultaneously requires defining a suitable cost function. We propose a cost function which has the form of

$$J = \int_0^T \alpha \cdot \frac{\dot{m}_f(t)}{M} + (1 - \alpha) \cdot \frac{\sigma(t) \cdot |I(t)|}{\Lambda} dt. \tag{13}$$

The first term represents fuel cost, while the second term can be interpreted as battery aging cost. The parameter α is a weighting factor which can take on any value between 0 and 1. One can continuously tradeoff between these two costs by varying the value of α, which should yield a Pareto front [23]. In order to make these two terms numerically comparable, normalization is needed for both. The key idea is to use a maximum instantaneous cost of one trip to normalize the actual cost. In the first term, M represents the maximum fuel flow rate in g/s, and in the second term, Λ is the maximum value of $\sigma(t) \cdot |I(t)|$ when only fuel consumption is considered in the optimization for a corresponding driving cycle.

Before trying to solve this optimization problem, one should recognize the fact that this is an optimal control problem subject to the dynamics described by

$$\dot{x} = -\frac{I(u, x)}{Q_{\mathrm{batt}}} \tag{14}$$

where x is SOC and u is the control input, i.e., the power flow within the electric machine $P_{\mathrm{em_{req}}}$. Thus, the optimal control problem takes the following mathematical form:

$$\begin{aligned} u^* &= \underset{u}{\operatorname{argmin}} : J \\ &\text{subject to} \\ \dot{x} &= -\frac{I(u,x)}{Q_{\mathrm{batt}}} \\ x(0) &= x_0 \\ x(T) &= x_0 \\ x(t) &\in \chi \\ u(t) &\in \mathcal{U} \end{aligned} \tag{15}$$

where χ and $\mathcal{U}$ are defined as the admissible state and control sets, respectively. As this control strategy is designed for charge sustaining HEVs, SOC at the end of one trip is required to equal to that at the beginning.

Among methods for solving optimal control problems, PMP is chosen to give numerical solution. According to PMP, minimizing the cost function in (13) is equivalent to minimizing the Hamiltonian

$$\begin{aligned} H(x(t),u(t),t) = \alpha \cdot \frac{\dot{m}_f(x,u)}{M} + (1-\alpha)\cdot\frac{\sigma(x,u)\cdot|I(x,u)|}{\Lambda} \\ + \lambda(t)\cdot\dot{x} \end{aligned} \tag{16}$$

where $\lambda(t)$ is the costate which evolves with the dynamics described by

$$\dot{\lambda}(t) = -\frac{\partial H(x(t),u(t),t)}{\partial x}. \tag{17}$$

The optimal control trajectory is given by

$$u^*(t) = \arg\min_{u\in\mathcal{U}} H(x^*(t),u(t),\lambda^*(t),t). \tag{18}$$

The initial value of costate $\lambda(t)$ can be determined by shooting method, if and only if *a priori* knowledge of the future driving condition is available [24].

IV. Regenerative Braking

One of the merits that HEVs have is the regenerative braking system which provides the ability to recover significant amount of energy during braking. Due to the fact that the vehicle works in either charge-sustaining mode or braking mode, regenerative braking can be controlled separately, which means the problem formulation in (15) does not include braking control. Basically, there are two brake control strategies: 1) series braking and 2) parallel braking [25], [26]. As battery aging is one of the main concerns in this work, energy recovered from regenerative braking is not free any more. Instead of using the basic brake control strategies, a static optimization-based regenerative braking control strategy is implemented so that an instantaneous decision is made on the distribution of total braking torque, which is optimally distributed between electric system and mechanical system. If the SOC level in the battery is beyond 0.65, only friction brake will be applied to prevent overcharging the battery. Usually, regenerative braking is effective only for the driven axle, which is the front axle in this study. As a result, the total braking torque request splits between the front axle and the rear axle according to the geometry of the vehicle. Then, the optimal regenerative braking is performed at the front axle. In order to consider both fuel economy and battery aging during regenerative braking, the following static optimization problem is solved

$$\begin{aligned} \min : \quad & \frac{P_{\mathrm{batt}}}{|P_{\mathrm{batt_{min_{regen}}}}|} + \frac{\sigma\cdot|I|}{I_{\mathrm{eff_{max_{regen}}}}} \\ \text{subject to} : \quad & P_{\mathrm{batt_{min}}} \leqslant P_{\mathrm{batt}} \leqslant 0 \\ & P_{\mathrm{em_{min}}} \leqslant P_{\mathrm{em}} \leqslant 0. \end{aligned} \tag{19}$$

During regeneration, battery power P_{batt} is negative, and we want to minimize this power to recuperate energy as much as possible. On the other hand, battery aging cost, which is represented by effective current $\sigma\cdot|I|$ needs to be minimized as well. Each of the two terms is normalized by the maximum absolute value during braking when only fuel economy is considered.

V. Engine Start–Stop

Another benefit of HEVs is the integration of engine start–stop function, which helps to save additional amount of fuel during vehicle standstill. Some results can be found where start–stop is an integral part of the energy management strategy design process [27], which is part of the future work, yet more often heuristic control is added to manage the ICE ON/OFF, which is the case in this work. The implemented rule-based start–stop strategy is as follows.

1) ICE OFF when vehicle speed is 0.
2) ICE ON when acceleration pedal is positive.

Fuel is cut off when acceleration pedal signal is 0. Every time the engine starts, it consumes a certain amount of fuel and electric power. Fuel cost for engine warm start is 100 mg; battery power requirement for engine start is 4.5 kW. The numbers were obtained from experimental data of the EcoCar2 prototype vehicle [27], which uses a 1.8-L Honda engine, the size of which is comparable to the one used in this work.

VI. Controller Implementation

The PMP states that the necessary conditions for the optimal control is

$$H(x^*(t),u^*(t),\lambda^*(t),t) \leqslant H(x^*(t),u(t),\lambda^*(t),t). \tag{20}$$

It is clear that before the optimal control solution can be determined, the costate should be solved appropriately, because the optimal state trajectory and costate trajectory are corresponding to each other. Basically this requires two steps. The first or key step is to implement the costate dynamics.

According to equation (17), the explicit form of the costate dynamics can be written as

$$\dot{\lambda}(t) = -\left(\frac{\alpha}{M}\cdot\frac{\partial \dot{m}_f(x,u)}{\partial x} + \frac{1-\alpha}{\Lambda}\cdot\frac{\partial \sigma(x,u)}{\partial x}\cdot|I(x,u)| + \frac{1-\alpha}{\Lambda}\cdot\sigma(x,u)\cdot\frac{\partial |I(x,u)|}{\partial x} + \lambda(t)\cdot\frac{\partial \dot{x}}{\partial x}\right) \tag{21}$$

in which the four terms describe the sensitivity of fuel flow rate, battery severity factor, the magnitude of battery current, and the rate of change in SOC with respect to SOC. The relationship between fuel flow rate and SOC is not directly clear, so the following transformation is made:

$$\frac{\partial \dot{m}_f(x,u)}{\partial x} = \frac{\partial \dot{m}_f(x,u)}{\partial P_{\rm em}(x)}\cdot\frac{\partial P_{\rm em}(x)}{\partial x}. \tag{22}$$

According to the assumption that the road power request should always be satisfied, the following equality holds:

$$\frac{\partial \dot{m}_f(x,u)}{\partial P_{\rm em}(x)} = \frac{\partial \dot{m}_f(x,u)}{\partial (P_{\rm road}-P_{\rm ice})} = -\frac{\partial \dot{m}_f(x,u)}{\partial P_{\rm ice}}. \tag{23}$$

Thus, complete costate dynamics can be expressed as

$$\dot{\lambda}(t) = -\left(-\frac{\alpha}{M}\cdot\frac{\partial \dot{m}_f(x,u)}{\partial P_{\rm ice}}\cdot\frac{\partial P_{\rm em}(x)}{\partial x} + \frac{1-\alpha}{\Lambda}\cdot\frac{\partial \sigma(x,u)}{\partial x}\cdot|I(x,u)| + \frac{1-\alpha}{\Lambda}\cdot\sigma(x,u)\cdot\frac{\partial |I(x,u)|}{\partial x} + \lambda(t)\cdot\frac{\partial \dot{x}}{\partial x}\right). \tag{24}$$

In this work, all the partial differential terms or sensitivities in (24) are precalculated and implemented as look-up tables in Simulink.

The second step is to search for an initial value of the costate, which is necessary to solve the differential equation in (24). Due to the fact that this optimal control problem is a two-point boundary problem with condition $x(0) = x(T) = x_0$, an iterative method, which is also known as shooting method [28], can be applied to search for the initial costate. In the simulation, the initial SOC is set to be 0.5, and the acceptable range of the final SOC is $0.49-0.51$.

VII. Simulation Results

In this work, four driving cycles are studied, and detailed results are presented for two of them, which are Federal Urban Driving Schedule (FUDS) and US06. All the cycles are replicated to fulfill the distance of 44 km, which is defined as one-day driving.

Inside the battery, chemical reactions are driven either by voltage or temperature [4]. The higher the temperature the battery undergoes, the faster the chemical reactions will occur and the higher the aging rate is as well. Given this fact, the ambient temperature is set to $40\,^{\circ}\mathrm{C}$, which is an extrema but still reasonable condition for a city like Phoenix in Arizona.

The virtual experiments are divided into two groups, namely short-term, which is one-day driving, and long-term simulations, which is one-year driving.

TABLE III
Short-Term Simulation Results FUDS

α	Final SOC	MPG	Effective Ah
0.3	0.50	45.1	17.5
0.5	0.50	45.3	17.9
0.7	0.50	45.4	18.2
0.9	0.50	45.5	19.2
1	0.50	45.8	22.9

A. Short-Term Simulation Results for FUDS

In the simulation, five different values of α are considered. According to the cost function in (13), when $\alpha = 1$, only fuel consumption is considered in the optimization, which should lead to the best fuel economy. On the other hand, when α decreases, battery aging is weighted more and more, thus less aging is expected. The short-term simulation results of FUDS are listed in Table III. The best fuel economy, which is 45.8 MPG, comes from the case in which $\alpha = 1$, while the least aging is obtained with $\alpha = 0.3$, in which the effective Ah-throughput is 17.5. When compared with the best fuel economy case, the effective Ah-throughput decreases by 23.6%; however, the fuel consumption increases only by 1.5%. When look into the performance of the electric motor, it is clearly indicated by the top plot in Fig. 5 that the case with $\alpha = 0.3$ tends to provide assist torque in a much more gentle way, while in the case of $\alpha = 1$, there are more frequent instances of high C-rate request from the battery. Fig. 4 shows the battery operating points on the severity factor map with $\alpha = 0.3$ on the top and $\alpha = 1$ on the bottom. The severity factors of $\alpha = 0.3$ are distributed lower than that of $\alpha = 1$ on the severity factor map in all modes, though $\alpha = 0.3$ has more instances of high severity factors in the assist mode. The rms values of severity factor corresponding to $\alpha = 0.3$ and $\alpha = 1$ are 3.1 and 3.4, respectively. Distribution of severity factors from $\alpha = 0.3$ is wider on the axes of SOC and especially located in lower SOC range. This can be explained by the aging model in (7), which means low SOC is preferred in terms of decreasing aging speed. As a result, with the same boundary conditions, which are $\mathrm{SOC}(0) = \mathrm{SOC}(T) = 0.5$, the controller with consideration of battery aging chooses to spend more time in low SOC level as long as all the constraints are respected. The SOC profiles for both cases are shown in the bottom plot of Fig. 5.

B. Short-Term Simulation Results for US06

The same analysis is conducted on the US06 driving schedule. As listed in Table IV, similar trend can be observed when α varies. Under aggressive driving conditions, the inclusion of the battery aging cost clearly results in a significant reduction in effective Ah-throughput. Fig. 6 shows the electric torque and SOC trajectories from both cases, and it is obvious that, in the case of $\alpha = 0.3$, the assist torque from electric machine is smaller than that in the case of $\alpha = 1$; the SOC trajectory corresponding to $\alpha = 0.3$ is mostly under the one with $\alpha = 1$, and the reason is as stated before. In Fig. 7, it is clear that severity factors are dramatically reduced in both regeneration

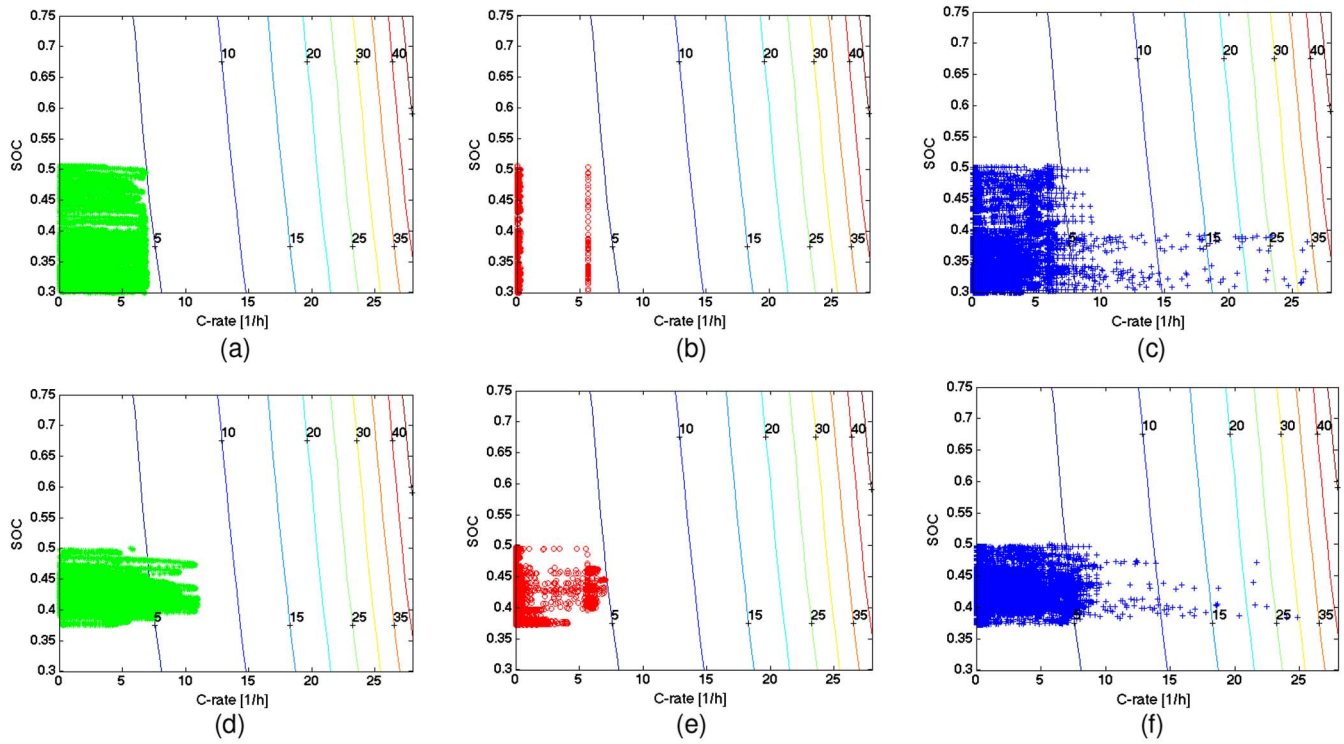

Fig. 4. Distribution of battery severity factor over FUDS. (a) $\alpha = 0.3$, Regeneration. (b) $\alpha = 0.3$, Charging. (c) $\alpha = 0.3$, Assist. (d) $\alpha = 1$, Regeneration. (e) $\alpha = 1$, Charging. (f) $\alpha = 1$, Assist.

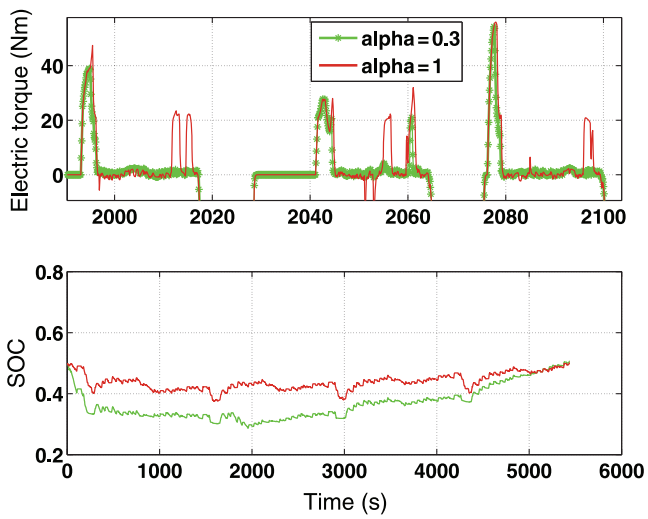

Fig. 5. Electric torque and SOC profiles over FUDS.

TABLE IV
SHORT-TERM SIMULATION RESULTS US06

α	Final SOC	MPG	Effective Ah
0.3	0.50	34.6	22.3
0.5	0.50	34.5	27.3
0.7	0.50	34.5	34.1
0.9	0.50	34.5	39.6
1	0.50	35.9	77.6

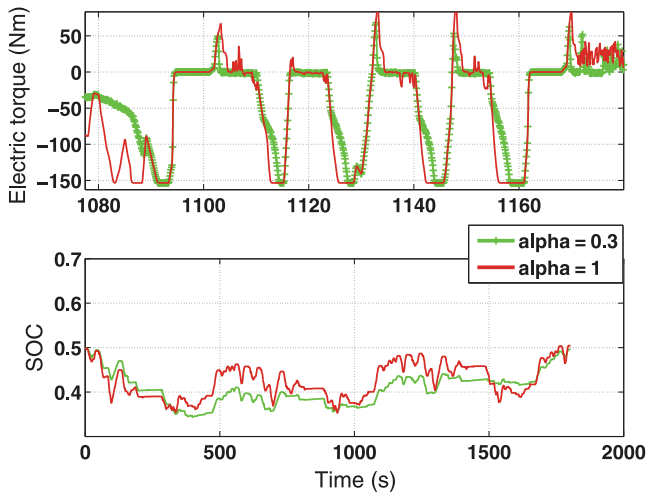

Fig. 6. Electric torque and SOC profiles over US06.

and charging modes with $\alpha = 0.3$. Though, in assist mode, the shape of severity factor distribution of the two cases is similar, the density distribution is different. With $\alpha = 0.3$, severity factors are mostly located below 20, while with $\alpha = 1$, the density of severity factor at high values becomes bigger. The rms values of severity factor corresponding to $\alpha = 0.3$ and $\alpha = 1$ are 5.5 and 10.6, respectively.

C. Summary of Short-Term Simulation Results

In Table V, short-term simulation results of four driving cycles are listed including FUDS and US06. Manhattan driving schedule is a very intense city cycle, while West Virginia Interstate represents highway driving conditions. Two values of α for each cycle are shown. According to the simulation results,

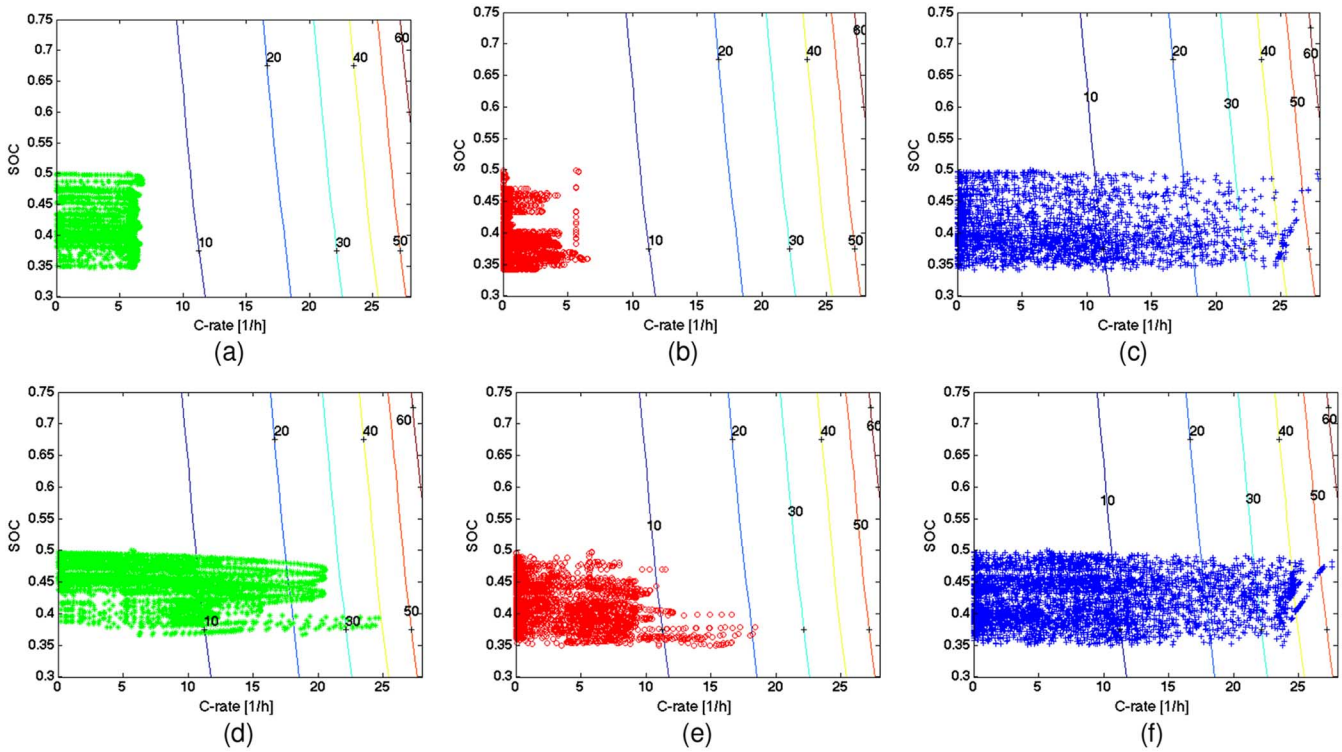

Fig. 7. Distribution of battery severity factor over US06. (a) $\alpha = 0.3$, Regeneration. (b) $\alpha = 0.3$, Charging. (c) $\alpha = 0.3$, Assist. (d) $\alpha = 1$, Regeneration. (e) $\alpha = 1$, Charging. (f) $\alpha = 1$, Assist.

TABLE V
SHORT-TERM SIMULATION SUMMARY

	FUDS		US06		Manhattan		WVU-inter	
α	MPG	$\mathrm{Ah_{eff}}$	MPG	$\mathrm{Ah_{eff}}$	MPG	$\mathrm{Ah_{eff}}$	MPG	$\mathrm{Ah_{eff}}$
0.3	45.1	17.5	34.6	22.3	28.3	27.4	49.8	2.65
1	45.8	22.9	35.9	77.6	28.7	45.4	49.9	7.98

the optimal controller with consideration of battery aging is able to dramatically reduce battery aging with almost negligible effect on fuel economy.

D. Long-Term Simulation Results

The long-term simulations focus on the trajectory of battery capacity degradation. The simulations are conducted under the following assumptions. 1) One-year simulation is equivalent to 365 one-day simulations. 2) Driving conditions are the same for each day, which means the driving cycle is repetitive and the ambient temperature $\theta = 40\,^{\circ}\mathrm{C}$. To have an idea of the battery degradation trajectory over 1 year under extreme conditions, $40\,^{\circ}\mathrm{C}$ is chosen for the whole year. In order to guarantee charge sustenance on each day, a searching algorithm is inserted to refresh the value of initial costate. The reason why charge sustenance may be violated is that battery capacity is reducing due to aging effect, which influences (14). With a degraded battery, the same initial costate will lead to a high final SOC, which may be located outside of the acceptable range.

Fig. 8 depicts the long-term simulation result for $\alpha = 0.3$ and $\alpha = 1$. It is clear that, due to the nature of the driving cycle, there is little opportunity to reduce the effective Ah-throughput.

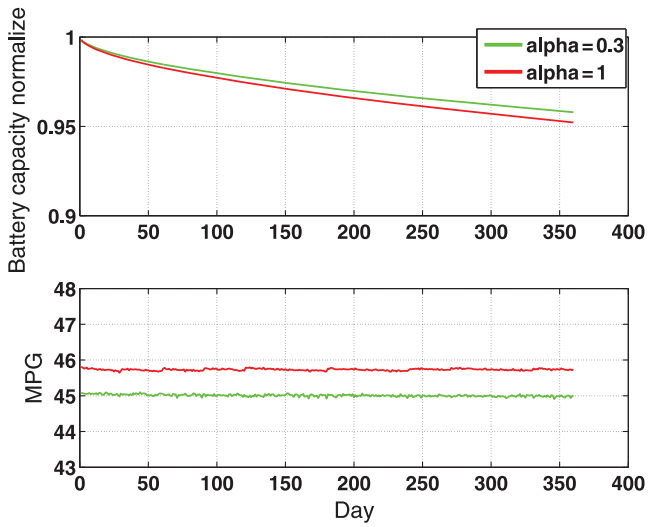

Fig. 8. One-year driving simulation FUDS.

Fig. 9 shows the instantaneous normalized aging costs without weighting factor, which can be mathematically expressed as

$$\mathrm{cost}_{\mathrm{aging}} = \frac{\sigma \cdot |I|}{\Lambda}. \tag{25}$$

It is obvious that the difference in the instantaneous aging cost between these two cases is minor. This duty cycle leads the battery operating points to the region in which the aging effect is not sensitive to control. According to Fig. 8, fuel economy is almost a constant for both values of α. The reason is that the

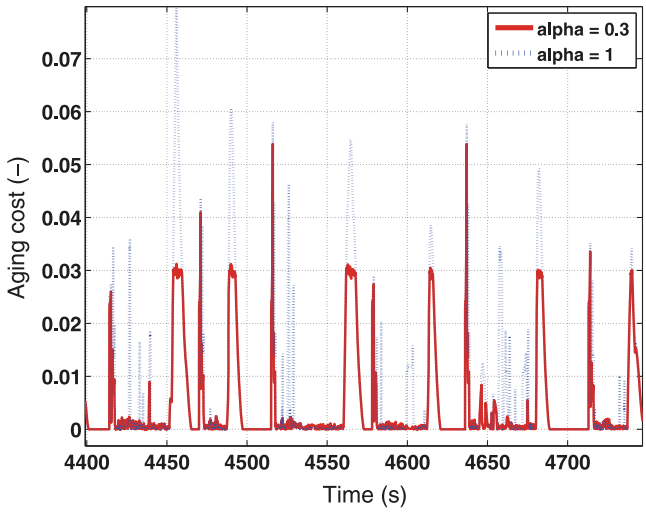

Fig. 9. Instantaneous aging cost over FUDS.

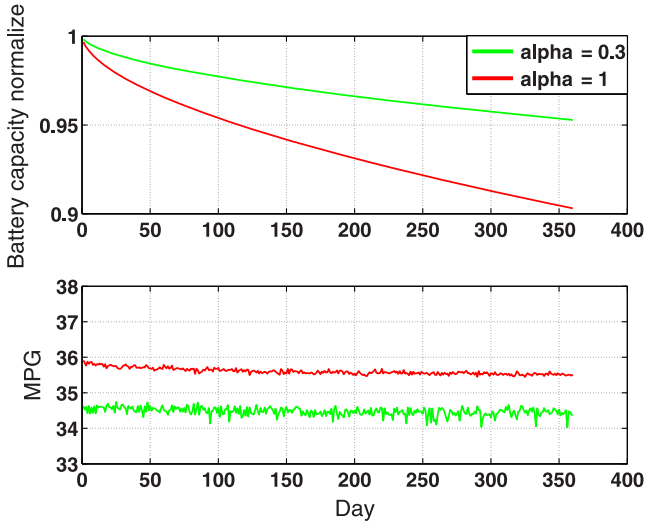

Fig. 10. One-year driving simulation US06.

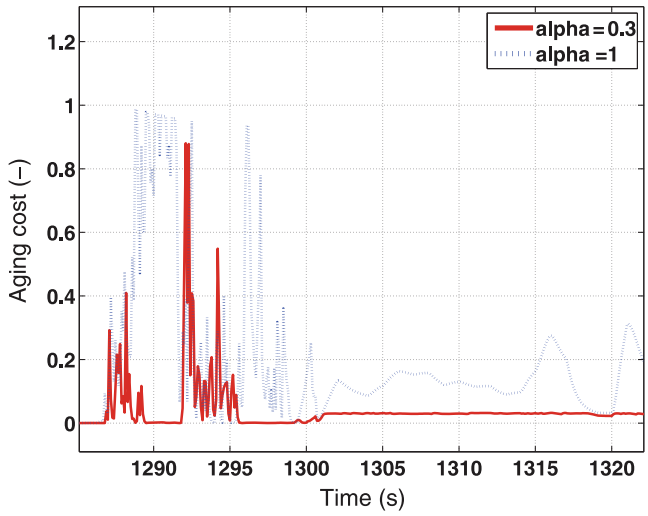

Fig. 11. Instantaneous aging cost over US06.

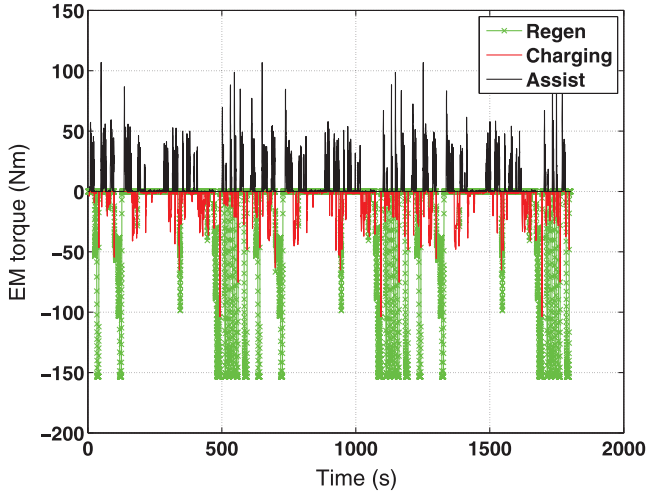

Fig. 12. Electric torque over US06, $\alpha = 1$.

capacity loss at the end of 1 year is not big enough to make a difference on fuel economy.

On the other hand, the long-term simulation results using US06 driving cycle, reported in Fig. 10, show very different battery capacity loss for different values of α. Fig. 11 describes the instantaneous aging costs, which justifies the long-term simulation results. This harsh driving cycle makes the battery aging behavior sensitive to control; therefore, in this situation, the presented optimal algorithm can significantly improve battery life.

E. Insights From Simulation Results

In the simulator used in this study, the PMP-based controller is functional only when the vehicle is in charge sustaining mode; regenerative braking is controlled separately. When aging is considered or when α is different from 1, regenerative braking strategy is the one stated in Section IV, which optimally trades off recuperated energy with battery aging. When $\alpha = 1$, a series regenerative braking strategy is implemented, which permits recovering the maximum possible amount of vehicle kinetic energy as long as the physical limits of the electric motor and battery are not violated. Regenerative braking has a potentially significant influence on battery aging; Fig. 12 shows the torque output from the electric machine over US06 with $\alpha = 1$, which clearly indicates that regenerative braking accounts for a large part of the battery usage. The results summarized in Table VI show that the change of effective Ah-throughput due to regenerative braking, for values of α different from 1, is minor, because the amount of braking energy that can be recovered is determined by the driving cycle and the control algorithm of braking, both of which are the same for these cases. However, when compared with the case of $\alpha = 1$, effective Ah-throughput is reduced significantly. On the other hand, the amount of energy recovered is also reduced, which contributes to the difference in fuel economy. In practice, the implementation of regenerative braking algorithm in a vehicle may differ from the way it was modeled in this study, and its effect on aging will depend on the braking strategy employed in the vehicle controller. It may be possible to further reduce battery aging by designing an appropriate braking strategy.

TABLE VI
BATTERY USAGE ON US06

α	Effective Ah	Effective Ah from Regen	Energy recovered (kJ)
0.3	22.3	5.3	1.3
0.5	27.3	5.5	1.3
0.7	34.2	5.6	1.3
0.9	39.6	5.7	1.3
1	77.6	23.6	2.3

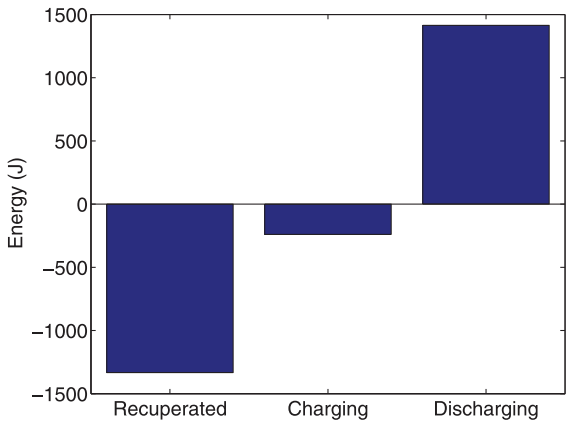

Fig. 13. Battery energy flow over US06, $\alpha = 0.3$.

TABLE VII
ENERGY ANALYSIS ON US06

Constraint	Recuperated (J)	Charging (J)	Discharging (J)
$T_{\text{regen}_{max}} = T_{em_{min}}$	1333	240	1414
$T_{\text{regen}_{max}} = \frac{2}{3}T_{em_{min}}$	1300	173	1384
$T_{\text{regen}_{max}} = \frac{1}{2}T_{em_{min}}$	1196	144	1278

Some insights on PMP-based solution can be gained by conducting energy analysis of the vehicle operation. According to the simulation results of Fig. 13, which shows the battery energy usage over US06 with $\alpha = 0.3$, the controller rarely uses the engine to charge the battery, for the stated operating conditions. In fact, the energy supplied to the battery by the engine is negligible when compared to that from regenerative braking. The optimal controller reveals that using the engine to recharge the battery is not cost-effective, because the sum of the fuel cost and effective Ah-throughput cost is too large. As a result, the controller, in the charge-sustaining mode, will only use the amount of energy that can be compensated by regenerative braking so that the requirement of charge sustenance can be satisfied. This fact is confirmed by the simulation results listed in Table VII, in which one can see that limiting the maximum allowable regenerative torque causes the energy recuperated from the braking to decrease accordingly. The energy discharged from the battery to assist the engine also decreases, and the discharged energy is almost equal to the recuperated energy. Because of the iterative nature of the PMP solution (using the shooting method to tune initial costate), the PMP optimal controller knows the future, and it finds the minimum fuel consumption by matching the amount

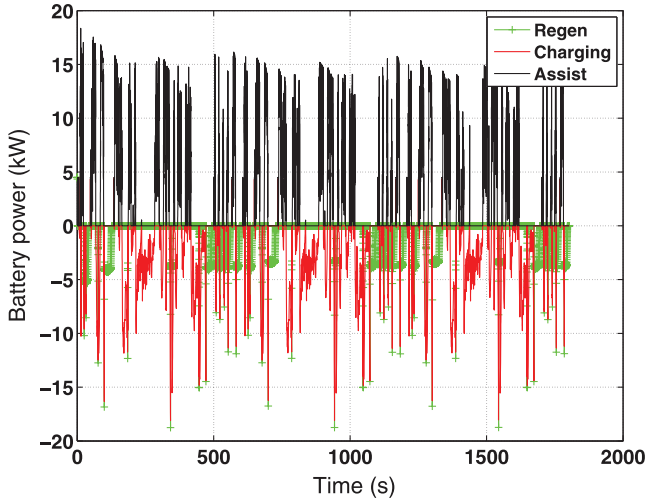

Fig. 14. Battery power with 1.0 L engine over US06, $\alpha = 0.3$.

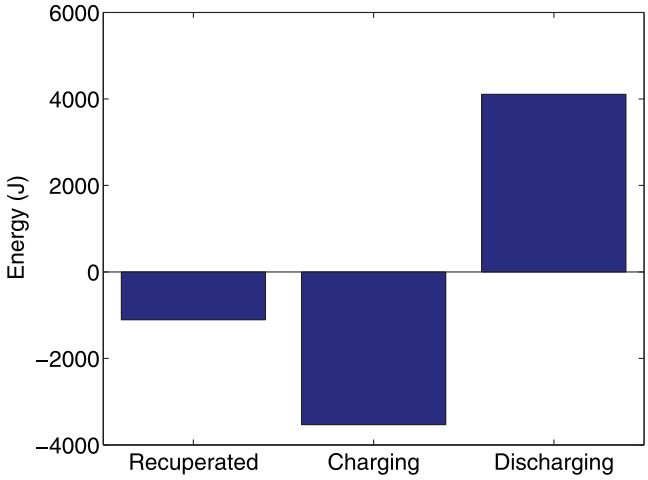

Fig. 15. Battery energy with 1.0 L engine over US06, $\alpha = 0.3$.

of energy that can be recovered from the regenerative braking with the positive battery power used for electric assist. Only occasionally is the fuel cost associated with recharging the battery from the engine considered acceptable in the PMP solution. Thus, recharging the battery with the ICE is an infrequent event. However, it is conceivable that with different powertrain configurations or in more aggressive driving, a greater amount of electric torque assist will be used in practice, requiring more ICE recharge. To validate this statement, a hybrid powertrain using a significantly downsized engine, 1.0 L in displacement, is tested in the simulation. The CVT control strategy is modified accordingly so that the OOL of the new engine can be tracked, while the remaining powertrain subsystems are unchanged. Figs. 14 and 15 show the simulation result of battery operating conditions over US06 driving cycle with $\alpha = 0.3$. It is obvious that with a smaller engine, the need for electric assist is much greater, and that more frequent charging events are required to meet the constraint of charge sustenance. As a result, the controller will use the engine to charge the battery more frequently. So the battery, with a smaller engine, is used in a much more intensive way.

TABLE VIII
VEHICLE PERFORMANCE WITH DIFFERENT ENGINE SIZE

Engine size	Final SOC	MPG	Effective Ah
1.6 Liter	0.50	34.6	22.3
1.0 Liter	0.49	35.7	144.0

It is also true that the fuel cost is lower because of the more favorable fuel economy features of the downsized engine. Table VIII summarizes the performance of the vehicle with two different engines over the US06 driving cycle with $\alpha = 0.3$. With aggressive engine downsizing, fuel economy is improved; however, the battery is used more aggressively as indicated by effective Ah-throughput. Overall, fuel savings are minor when compared with the dramatic increase in battery aging cost. Design optimization studies that selecting optimal component sizing to optimally trade off fuel economy and performance in hybrid electric and plug-in HEVs have been widely reported in the past [29]–[33]. It has been clearly shown that both the energy consumption and the vehicle performance are linked to the size of the powertrain components in a hybrid vehicle [34]–[38], and that there exists an optimal powertrain configuration that yields the best combination of vehicle performance and cost for a given cost function. The work presented in this paper clearly shows that including battery life in the cost function used to perform such a design optimization is very important, and adds a critical dimension to the design of an HEV. The optimal controller presented in this paper is a useful tool in carrying out such design optimization studies.

VIII. CONCLUSION AND FUTURE WORK

This paper has analyzed an optimal control-based energy management strategy for HEVs, which explicitly trades off fuel consumption and battery capacity degradation. The optimal controller explicitly uses a battery aging model. The methods developed in this paper provide significant insights into the tradeoff between fuel economy and battery aging in an HEV. While the specific models and results will vary with battery chemistry and vehicle architecture, the models and optimal control algorithms developed in this study show that it is possible to explicitly take into account battery aging in an energy management controller, with the potential to significantly extend battery life when the vehicle is operated in various conditions, without adversely affecting performance, and with a very small penalty in fuel economy. The work presented in this paper forms the basis for the future study of the optimal behavior including regeneration and engine start–stop as well as the design of causal control algorithms that can be implemented and calibrated on board a vehicle.

REFERENCES

[1] S. S. Choi and H. S. Lim, "Factors that affect cycle-life and possible degradation mechanisms of a Li-ion cell based on LiCoO2," *J. Power Sources*, vol. 111, no. 1, pp. 130–136, 2002.

[2] J. Vetter *et al.*, "Ageing mechanisms in lithium-ion batteries," *J. Power Sources*, vol. 147, no. 1, pp. 269–281, 2005.

[3] M. Broussely *et al.*, "Main aging mechanisms in Li-ion batteries," *J. Power Sources*, vol. 146, no. 1, pp. 90–96, 2005.

[4] J. R. Belt, C. D. Ho, T. J. Miller, M. A. Habib, and T. Q. Duong, "The effect of temperature on capacity and power in cycled lithium ion batteries," *J. Power Sources*, vol. 142, no. 1, pp. 354–360, 2005.

[5] J. Wang *et al.*, "Cycle-life model for graphite-$LiFePO_4$ cells," *J. Power Sources*, vol. 196, no. 8, pp. 3942–3948, 2011.

[6] S. J. Moura, J. L. Stein, and H. K. Fathy, "Battery-health conscious power management for plug-in hybrid electric vehicles via stochastic control," in *Proc. ASME Conf. Dyn. Syst. Control Conf.*, 2010, pp. 615–624.

[7] L. Serrao, S. Onori, A. Sciarretta, Y. Guezennec, and G. Rizzoni, "Optimal energy management of hybrid electric vehicles including battery aging," in *Proc. Amer. Control Conf. (ACC)*, 2011, pp. 2125–2130.

[8] S. Ebbesen, P. Elbert, and L. Guzzella, "Battery state-of-health perceptive energy management for hybrid electric vehicles," *IEEE Trans. Veh. Technol.*, vol. 61, no. 7, pp. 2893–2900, Sep. 2012.

[9] T. M. Padovani *et al.*, "Optimal energy management strategy including battery health through thermal management for hybrid vehicles," *Adv. Automot. Control*, vol. 7, no. 1, pp. 384–389, 2013.

[10] G. Rizzoni, L. Guzzella, and B. M. Baumann, "Unified modeling of hybrid electric vehicle drivetrains," *IEEE/ASME Trans. Mechatron.*, vol. 4, no. 3, pp. 246–257, Sep. 1999.

[11] B. Bonsen, M. Steinbuch, and P. Veenhuizen, "CVT ratio control strategy optimization," in *Proc. IEEE Conf. Veh. Power Propul.*, 2005, vol. 9, pp. 227–231.

[12] J. Marcicki, F. Todeschini, S. Onori, and M. Canova, "Nonlinear parameter estimation for capacity fade in lithium-ion cells based on a reduced-order electrochemical model," in *Proc. Amer. Control Conf.*, 2012, pp. 572–577.

[13] J. Marcicki, G. Rizzoni, A. Conlisk, and M. Canova, "A reduced-order electrochemical model of lithium-ion cells for system identification of battery aging," in *Proc. ASME Dyn. Syst. Control Conf. Bath/ASME Symp. Fluid Power Motion Control*, 2011, pp. 709–716.

[14] P. Ramadass, B. Haran, P. M. Gomadam, R. White, and B. N. Popov, "Development of first principles capacity fade model for Li-ion cells," *J. Electrochem. Soc.*, vol. 151, no. 2, pp. A196–A203, 2004.

[15] I. Bloom *et al.*, "An accelerated calendar and cycle life study of Li-ion cells," *J. Power Sources*, vol. 101, no. 2, pp. 238–247, 2001.

[16] A. Cordoba-Arenas, S. Onori, Y. Guezennec, and G. Rizzoni, "Capacity and power fade cycle-life model for plug-in hybrid electric vehicle lithium-ion battery cells containing blended spinel and layered-oxide positive electrodes," *J. Power Sources*, vol. 278, pp. 473–483, 2015.

[17] J. Groot, "State-of-health estimation of Li-ion batteries: Cycle life test methods," M.S. thesis, Div. Electric Power Eng., Dep. Energy Environ., Chalmers Univ. Technology, Göteborg, Sweden, 2012.

[18] P. Spagnol, S. Onori, N. Madella, Y. Guezennec, and J. Neal, "Aging and characterization of Li-ion batteries in a HEV application for lifetime estimation," in *Proc. IFAC Symp. Adv. Automot. Control*, 2010.

[19] G. Suri and S. Onori, "A control-oriented Li-ion battery aging model for hybrid electric vehicle optimization," *Energy*, 2015.

[20] L. Serrao, S. Onori, G. Rizzoni, and Y. Guezennec, "Model based strategy for estimation of the residual life of automotive batteries," in *Proc. 7th IFAC Symp. Fault Detect. Superv. Saf. Tech. Processes (SAFEPROCESS'09)*, 2009, pp. 923–928.

[21] S. Onori, P. Spagnol, V. Marano, Y. Guezennec, and G. Rizzoni, "A new life estimation method for lithium–ion batteries in plug–in hybrid electric vehicles applications," *Int. J. Power Electron.*, vol. 4, no. 3, pp. 302–319, 2012.

[22] V. Marano, S. Onori, Y. Guezennec, G. Rizzoni, and N. Madella, "Lithium-ion batteries life estimation for plug-in hybrid electric vehicles," in *Proc. IEEE Conf. Veh. Power Propul. Conf.*, 2009, pp. 536–543.

[23] R. T. Marler and J. S. Arora, "Survey of multi-objective optimization methods for engineering," *Struct. Multidiscip. Optim.*, vol. 26, no. 6, pp. 369–395, 2004.

[24] D. E. Kirk, *Optimal Control Theory: An Introduction*. New York, NY, USA: Dover, 2012.

[25] E. Mehrdad, Y. Geo, and A. Emadi, *Modern Electric, Hybrid Electric, and Fuel Cell Vehicles: Fundamentals, Theory, and Design*, 2nd ed. Boca Raton, FL, USA: CRC, 2010.

[26] F. Sangtarash, V. Esfahanian, H. Nehzati, S. Haddadi, M. A. Bavanpour, and B. Haghpanah, "Effect of different regenerative braking strategies on braking performance and fuel economy in a hybrid electric bus employing cruise vehicle simulation," SAE Tech. Paper, Tech. Rep. 2008-01-1561, 2008.

[27] J. Ward, "Reduction of startup emissions for an alternative fueled engine," B.S. thesis, Dep. Mech. Aerosp. Eng., Ohio State Univ., Columbus, OH, USA, 2013.

[28] L. Serrao, S. Onori, and G. Rizzoni, "A comparative analysis of energy management strategies for hybrid electric vehicles," *J. Dyn. Syst. Meas. Control*, vol. 133, no. 3, p. 031012, 2011.

[29] T. Miller, G. Rizzoni, and Q. Li, "Simulation-based hybrid-electric vehicle design search," SAE Tech. Paper No. 1999-01-1150, 1999.
[30] R. Fellini, N. Michelena, P. Papalambros, and M. Sasena, "Optimal design of automotive hybrid powertrain systems," in *Proc. 1st Int. Symp. Environ. Conscious Des. Inverse Manuf.*, 1999, pp. 400–405.
[31] D. Assanis *et al.*, "Optimization approach to hybrid electric propulsion system design," *J. Struct. Mech.*, vol. 27, no. 4, pp. 393–421, 1999.
[32] W. Gao and S. K. Porandla, "Design optimization of a parallel hybrid electric powertrain," in *Proc. IEEE Conf. Veh. Power Propul.*, 2005, 6 pp.
[33] X. Wu, B. Cao, X. Li, J. Xu, and X. Ren, "Component sizing optimization of plug-in hybrid electric vehicles," *Appl. Energy*, vol. 88, no. 3, pp. 799–804, 2011.
[34] G. Rizzoni *et al.*, "Modeling, simulation, and concept design for hybrid-electric medium-size military trucks," in *Proc. SPIE Def. Secur. Symp.*, 2005, pp. 1–12.
[35] P. Pisu *et al.*, "Evaluation of powertrain solutions for future tactical truck vehicle systems," in *Proc. SPIE Def. Secur. Symp.*, 2006, pp. 62280D–62280D.
[36] T. Donateo, L. Serrao, and G. Rizzoni, "A two-step optimisation method for the preliminary design of a hybrid electric vehicle," *Int. J. Electr. Hybrid Veh.*, vol. 1, no. 2, pp. 142–165, 2008.
[37] R. Patil, B. Adornato, and Z. Filipi, "Design optimization of a series plug-in hybrid electric vehicle for real-world driving conditions," *SAE Int. J. Engines*, vol. 3, no. 1, pp. 655–665, 2010.
[38] N. Murgovski, L. Johannesson, J. Sjöberg, and B. Egardt, "Component sizing of a plug-in hybrid electric powertrain via convex optimization," *Mechatronics*, vol. 22, no. 1, pp. 106–120, 2012.

Li Tang (GSM'15–M'15) received the B.S. degree in mechanical engineering from Shandong University, Jinan, China, in 2010, and the M.S. degree in mechanical engineering from Carnegie Mellon University, Pittsburgh, PA, USA, in 2012. She is working toward the Ph.D. degree in mechanical and aerospace engineering at Ohio State University, Columbus, OH, USA.

Currently, she is a Graduate Research Associate with the Center of Automotive Research, Department of Mechanical and Aerospace Engineering, Ohio State University. Her research interests include dynamic system, optimal control, and energy management of hybrid electric vehicles.

Giorgio Rizzoni (S'83–M'85–SM'02–F'04) received the B.S., M.S., and Ph.D. degrees from the University of Michigan, Ann Arbor, MI, USA, in 1980, 1982, and 1986, respectively, all in electronics and communication engineering.

He is the Chair of Ford Motor Company in ElectroMechanical Systems. He is a Professor of Mechanical and Aerospace Engineering and Electrical and Computer Engineering with the Ohio State University (OSU), Columbus, OH, USA. Since 1999, he has been the Director of the Center for Automotive Research (CAR), Ohio State University, an interdisciplinary university research center in the OSU College of Engineering. He has contributed to the development of graduate curricula in these areas, and has served as the Director of three U.S. Department of Energy Graduate Automotive Technology Education Centers of Excellence: Hybrid Drivetrains and Control Systems from 1998 to 2004, Advanced Propulsion Systems from 2005 to 2011, and Energy Efficient Vehicles for Sustainable Mobility from 2011 to 2016. Since January 2011, he has been the OSU Site Director for the U.S. Department of Energy China-USA Clean Energy Research Center-Clean Vehicles. His research interests include modeling, control and diagnosis of advanced vehicles, energy efficiency, alternative fuels, the interaction between vehicles and the electric power grid, vehicle safety and intelligence, and policy and economic analysis of alternative fuels and vehicle fuel economy.

Prof. Rizzoni is a Fellow of SAE in 2005. He was the recipient of the 1991 National Science Foundation Presidential Young Investigator Award, and of several other technical and teaching awards.

Simona Onori (M'08) received the Laurea degree (*summa cum laude*) in computer engineering from the University of Rome Tor Vergata, Rome, Italy, in 2003, the M.S. degree in electrical and computer engineering from the University of New Mexico, Albuquerque, NM, USA, in 2004, and the Ph.D. degree in control engineering from the University of Rome Tor Vergata, in 2007.

Prior to joining the Department of Automotive Engineering, Clemson University, Greenville, SC, USA, she was a Research Scientist with the Center for Automotive Research, Ohio State University (OSU), Columbus, OH, and a Lecturer with the Mechanical and Aerospace Engineering Department, OSU, where she taught at undergraduate and graduate levels. She also previously worked with IBM, Rome, Italy from 2000 to 2002 and Thales-Alenia Space, Rome, Italy, in 2007. Her research has been funded by, among others, Fiat Chrysler Automobiles (FCA), BorgWarner, Honda, General Motors, Cummins, the National Science Foundation, and the U.S. Department of Energy. Her background is in control system theory, and her research interests include ground vehicle propulsion systems, energy storage systems, after treatment systems, with an emphasis on modeling, simulation, optimization, and feedback control design.

Dr. Onori is a member of American Society of Mechanical Engineers (ASME), Society of Automotive Engineers (SAE), and International Federation of Automatic Control (IFAC). She is the Chair of the IEEE Control Systems Society (CSS) Technical Committee on Automotive Controls from 2015 to 2017 and the Vice Chair of the IFAC Technical Committee on Automotive Controls. She is in the Editorial Board of *Engine and Automotive Engineering,* a speciality of *Frontiers in Mechanical Engineering,* and *SAE International Journal of Advanced Powertrains*. She was the recipient of the 2012 Lumley Interdisciplinary Research Award from the OSU College of Engineering and the TechColumbus 2011 Outstanding Technology Team Award.